JOURNAL OF MATERIALS SCIENCE 33 (1998) 5665–5669

Synthesis of germanium nanocrystals in SiO_2

J. G. COUILLARD, H. G. CRAIGHEAD*
*Department of Materials Science and Engineering, and *School of Applied and Engineering Physics, Cornell University, Ithaca, NY 14853, USA*
E-mail: couillarjg@corning.com

Germanium nanocrystals in SiO_2 with an average diameter of 5–25 nm were fabricated by co-deposition and annealing at 700–1000 °C. X-ray diffraction and transmission electron microscopy were used to measure the nanocrystal growth as a function of anneal time and temperature. The precipitation of nanocrystals was found not to follow the theory for precipitation from a solid solution of Lifshitz–Slezov; nanocrystal growth appears instead to be determined primarily by anneal temperature with little anneal time dependence. This departure from theory is attributed to the high concentration (40 at %) of germanium in the deposited films. A modified log-normal distribution was found to describe the distribution of nanocrystal sizes best. Photoluminescence was observed from nanocrystal-containing films, with luminescence energy shifted from that of bulk germanium. The luminescence spectra are in agreement with the theory of Brus for quantum confined carriers in small semiconductor crystals.

1. Introduction

Semiconductor nanocrystals have attracted interest in recent years, due to their exhibition of novel optical phenomena. These crystals provide a good mechanism for studying zero-dimensional quantum confinement effects, and their unusual optical properties may also be useful in fabricating optical devices. Recently researchers have investigated nanocrystals of group IV elements, such as silicon [1–4]. Silicon nanocrystals are interesting due to the similarity in the optical properties of silicon nanocrystals and porous silicon [5, 6].

Germanium nanocrystals are less widely studied [7–11]. Nevertheless, germanium makes a good candidate for the study of zero-dimensional systems. Being a group IV element, germanium can be readily incorporated into silicon systems and technologies. Importantly, because germanium has a larger dielectric constant and smaller carrier effective masses, the band structure of germanium is expected to be even more sensitive to size effects than that of silicon [12].

Other researchers have investigated the optical properties of germanium nanocrystals embedded in SiO_2 films. They have noted a shift in the optical absorption edge for small particles [7, 11], and some have observed luminescence suggestive of quantum confinement [8, 9]. Quantum efficiencies of 0.5% have been recorded from such samples at room temperature [10]. However, few comprehensive studies have been done exploring the formation and growth of germanium nanocrystals, their size distribution, and size distribution dependence of the luminescence [12].

In this study, we examined germanium nanocrystals in SiO_2 films fabricated by co-deposition and annealing. X-ray diffraction and transmission electron microscopy (TEM) were used to measure the nanocrystal sizes and determine their crystal phase. The nanocrystal growth was correlated to the anneal conditions. Photoluminescence (PL) at visible wavelengths from germanium nanocrystals was measured and compared with the predictions of quantum confinement theory.

2. Experimental procedure

2.1. Sample preparation

The growth technique used in this study was co-deposition of SiO_2 and germanium, followed by a high-temperature anneal. Pure germanium and SiO_2 sources in a high vacuum chamber were evaporated by heating with a focused electron beam. The evaporated materials were deposited together on a Si (1 0 0) substrate. Crystal monitors allowed the thickness of the film and the relative fraction of the two components to be controlled. The germanium concentration was 40 at % of the resulting film. Afterwards, samples were annealed at temperatures of 700–1000 °C for 30–180 min. This anneal step enables the germanium to diffuse within the relatively stable oxide matrix, and coalesce into increasingly larger crystals.

The annealing furnace consisted of a quartz tube enclosed in a resistive heater. The annealing gas used was moist hydrogen. This gas was chosen to satisfy the thermodynamic requirements of the desired samples. When SiO_2 sources are used in a vacuum deposition system, the resulting film is often not stoichiometric. The film is SiO_x, with $1 < x < 2$. This can complicate optical experiments, as non-stoichiometric silicon oxides are known to luminesce [13, 14]. Moist hydrogen can be used as the annealing gas to restore the oxygen content of the SiO_x to SiO_2 without converting the germanium to GeO_2 [8]. Rutherford backscattering (RBS) analysis on oxide samples after annealing indicates the oxide was stoichiometric to within the accuracy of the

technique. No elements other than germanium, silicon and oxygen were detected in any of the analyses performed on the films, although RBS is not sensitive to the presence of hydrogen. To determine whether hydrogen has been incorporated into the films accurately, a technique such as Fourier transform infrared spectroscopy (FTIR) would be required.

2.2. X-ray diffraction and TEM

X-ray diffraction offers a quick and non-destructive way to determine the nature of the germanium within the film. By examining samples with X-ray diffraction, the presence of crystalline phases can be verified, and conclusions drawn about the crystallography of any nanocrystals. It is also possible to estimate the size of the nanocrystals from the X-ray diffraction data. The theory of Scherrer relates the crystal size to broadening of the diffraction peak [15]. Other researchers have treated the Scherrer relation as being roughly comparable to the actual crystal size [16]. However, we have found that the Scherrer diameter determined from X-ray diffraction measurements is considerably larger than that seen by TEM.

The Scherrer equation was derived by considering a single crystal (or collection of crystals of equal size) as the diffraction source. In our samples, there is a broad distribution of crystal sizes. Larger crystals are expected to produce stronger diffraction signals, so the observed diffraction from a sample is thus produced primarily by its larger crystals. In estimating average crystal size from the observed diffraction signal the result is therefore artificially large. Computer simulations of this volume averaging effect using TEM crystal size data reproduced the large crystal sizes indicated from X-ray diffraction. X-ray diffraction is more useful for evaluating trends as a proportional measure of nanocrystal sizes. Transmission electron microscopy was used to obtain a more direct measurement of crystal sizes, and for collecting information about the distribution of crystal sizes.

2.3. Photoluminescence

PL measurements were performed on nanocrystalline germanium samples using a custom-built apparatus. The light source was an argon laser, operating at 488 nm with a maximum power of approximately 1 W. The laser light was directed through an optical chopper operating at 160 Hz and focused onto the sample surface. The sample was at room temperature. Specularly reflected laser light was directed into a beam stop, and re-emitted light from the sample was collected by a lens and directed to the detecting systems.

The sample luminescence was filtered through a half-meter grating monochrometer to select a wavelength, and the light collected by a photomultiplier tube. The signal from the photomultiplier tube was boosted using a current preamplifier, and directed to a lock-in amplifier using the chopper frequency as a reference.

To ensure consistency of the results, the monochrometer was calibrated to 632.8 nm between samples using a HeNe laser. The laser power was monitored using the PL peak from the band edge luminescence of a GaAsP reference sample at around 651 nm. Although our PL apparatus is not capable of measuring absolute quantum efficiencies, the observed luminescence from germanium nanocrystal samples was typically 100 times weaker than that of the GaAsP reference sample.

3. Results and discussion

3.1. Crystal growth

Samples were analysed using X-ray and electron diffraction, verifying that germanium was present in crystalline form. This is known because X-ray reflections were observed at the angles associated with germanium lattice planes. The relative intensities of the reflections at various lattice directions from the film are consistent with those from a germanium powder diffraction, suggesting that the germanium nanocrystals are in random orientation within the film.

Earlier claims by other researchers attributed luminescence from germanium nanocrystals to a tetragonal form of germanium [10, 17, 18]. As these alternate forms are only observed at particle dimensions less than 4 nm in diameter, they would produce faint and broad diffraction patterns. Such weak signals make it difficult to rule out the presence of alternate phases completely; however, no diffraction corresponding to anything other than normal germanium was ever detected from our X-ray and electron diffraction measurements. The lack of reflections at other angles also indicates that no other materials (such as silicon) are crystallizing in the films.

The theory of nanocrystal precipitation from a supersaturated solid solution was developed by Lifshitz and Slezov [19, 20]. They calculated a relationship between the average nanocrystal size, anneal time and anneal temperature as follows

$$\bar{R} \propto t^{1/3} \exp(-E/3kT) \tag{1}$$

where $\bar{R}$ is the nanocrystal size, t the anneal time, and T the anneal temperature. The Boltzmann constant, k, is known, and the activation energy, E, comes from the germanium diffusion constant. The crystal size distribution, $P(u)$, is also calculated to be

$$P(u) = \begin{cases} \dfrac{3^4 e}{2^{5/3}} \dfrac{u^2 \exp[-1/(1-2u/3)]}{(u+3)^{7/3}(3/2-u)^{11/3}} & u < 3/2 \\ 0 & u > 3/2 \end{cases} \tag{2}$$

where u is a dimensionless variable, with $u = 1$ the average crystal size; and e is the natural logarithm base.

Some of the germanium crystal sizes obtained from X-ray diffraction data are plotted in Fig. 1. The match to Lifshitz–Slezov growth theory is poor. There is almost no dependence of the crystal size on the anneal time, whereas Equation 1 predicts that the average size should increase with the cube root of the anneal time. This suggests that the crystals are reaching an

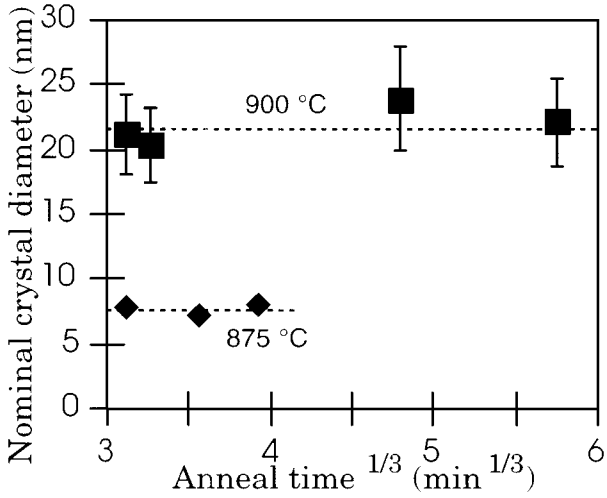

Figure 1 Crystal size (as estimated using X-ray diffraction) as a function of anneal time for two anneal temperatures. The dashed lines are fits to no time dependence.

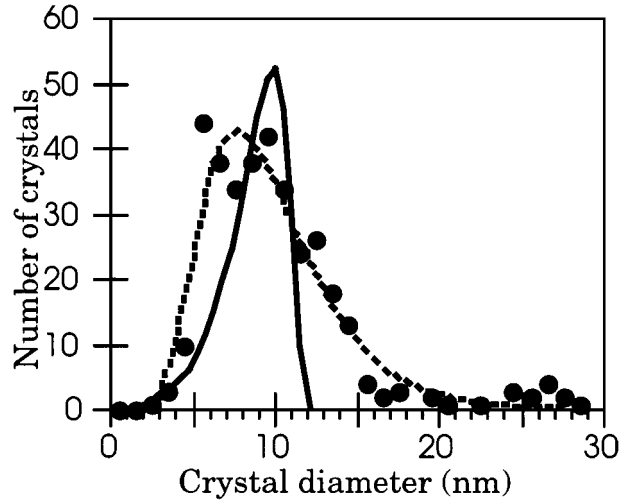

Figure 3 Distribution of germanium nanocrystal sizes, as determined from TEM micrographs. 367 crystals are included in the graph. Fits are to distribution functions as described in the text.

equilibrium size, which is determined primarily by the anneal temperature.

The $t^{1/3}$ time dependence has been experimentally observed in the precipitation of nanocrystals of compound semiconductors [21]. Hayashi *et al.* [7] noted a $t^{1/3}$ time dependence for annealing of germanium in SiO_2 at low concentrations (5 at %), whereas Maeda [12], working with higher germanium concentrations (42–46 mol %), did not. Maeda used argon as an annealing gas, and attributed the deviation from the growth theory to reduction of GeO_2 by excess silicon atoms. The choice of moist hydrogen as our annealing gas should prevent the formation of GeO_2. We believe the deviation from Lifshitz–Slezov growth theory results from their assumption that the distance between nanocrystals is much larger than the crystal size, which is not the case for such high germanium concentrations [21, 22].

In bright field TEM images, germanium crystals are clearly visible in the amorphous matrix. Fig. 2 is a bright field TEM image of a germanium nanocrystal sample

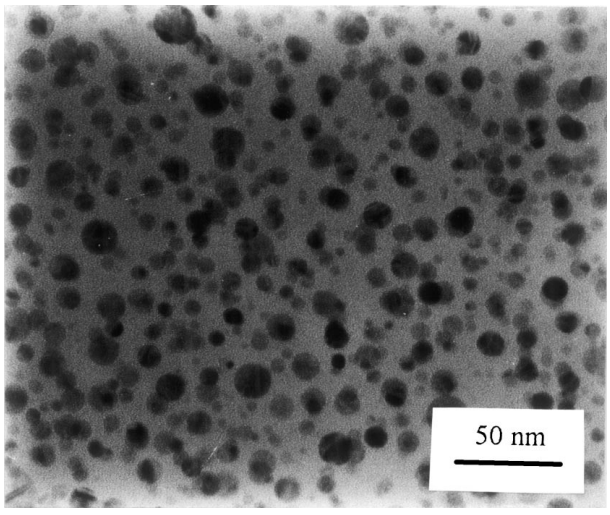

Figure 2 Bright field TEM image of a nanocrystal sample. The dark regions are crystalline, and correspond to germanium nanocrystals. The light background is amorphous SiO_2.

with average crystal diameter 11 nm and standard deviation of 3.4 nm. Nanocrystal sizes can be directly measured from bright field images to determine the crystal size distribution. A typical example of the crystal size distribution is given in Fig. 3. The Lifshitz–Slezov distribution function of Equation 2, shown in Fig. 3 as the solid line, is a poor fit to experimental data for this material system.

Empirical distributions are often used to fit nanocrystal size data. The log-normal function, a Gaussian of a logarithmic variable, is commonly used to describe systems with a fixed minimum (in our case zero crystal size) but no upper bound. The most commonly and successfully used distribution function for describing nanocrystal sizes is a modified log-normal distribution [23]

$$\frac{e^{\sigma^2}}{\sigma(2\pi)^{1/2}} \exp\left[-\frac{(\ln u + 3\sigma^2/2)^2}{2\sigma^2}\right] \qquad (3)$$

In Equation 3, u is the dimensionless size variable and σ the deviation. This distribution function is also plotted as a dotted line in Fig. 3, where it can be seen to match the experimental data quite well.

3.2. Photoluminescence

Argon laser light, when absorbed by semiconductor nanocrystals, is of high enough energy to generate an electron–hole pair. Recombination of these carriers, and the energy they emit as light, results in the observed PL. In a sufficiently small crystal, the generated carriers will feel a quantum confinement similar to the "particle in a box" of elementary quantum mechanics. Convenient units for energy and size at this scale are the effective Rydberg energy

$$E_{\mathrm{Ry}} = \frac{\mu e^4}{2\kappa^2\varepsilon^2\hbar^2} \qquad (4)$$

which represents the binding energy of the electron–hole pair, and the effective Bohr radius

$$a_{\mathrm{B}} = \frac{\kappa \varepsilon \bar{h}^2}{\mu e^2} \tag{5}$$

which is a measure of the average distance between the two charges [24]. Here κ is the Coulomb constant (1.11×10^{-10} C^2 Nm^{-2}), ε is the dielectric constant of the semiconductor (16.0 for germanium [25]), e the charge on the electron (1.602×10^{-19} C), $\bar{h}$ Planck's constant (1.055×10^{-34} J s), and μ the reduced mass, $1/\mu = 1/m_{\mathrm{h}} + 1/m_{\mathrm{e}}$. The masses m_{e} and m_{h} refer to the effective masses of electrons ($m_{\mathrm{e}} = 9.11 \times 10^{-28}$ g) and holes. Calculated reduced masses for germanium are $\mu_{\mathrm{lh}} = 0.021\ m_{\mathrm{e}}$ and $\mu_{\mathrm{hh}} = 0.036\ m_{\mathrm{e}}$ for the electron–light hole and electron–heavy hole excitons, respectively [12].

Experimentally the effective Rydberg energy for germanium is found to be 4.15 meV, corresponding to an effective Bohr radius of 11 nm [26, 27]. Calculated values of the effective Bohr radius in germanium can be as high as 38 nm [12]. Since the Bohr radius is much larger than the lattice spacing (0.566 nm in germanium), the use of effective masses is appropriate [24]. It has been established theoretically that the effective mass approximation is valid for crystals containing as few as 100 atoms [28].

For crystals much larger than the effective Bohr radius, neither electron nor hole should feel significant confinement energy. However, as the crystal size is reduced and the charges are forced together each will feel the energy shift appropriate to a particle in a well, as well as Coulomb attraction between them. The energy of the pair can be written as

$$E = E_{\mathrm{gap}} + \frac{\bar{h}^2}{2\mu}\left(\frac{\pi}{R}\right)^2 - 1.786\frac{e^2}{\varepsilon R} - 0.248E_{\mathrm{Ry}} \tag{6}$$

where R is the crystal radius.

The first two terms in Equation 6 are the quantized energy of confinement within a potential well. Éfros and Éfros theorized that electron–hole pairs in a semiconductor crystal should feel confinement proportional to R^{-2}, shortly after nanocrystal luminescence was first observed experimentally [29]. This confinement energy represents the deviations of the lowest electron state and the highest hole state from their energies in a bulk solid, where they are separated by E_{gap}. For germanium, E_{gap} is approximately 0.67 eV at room temperature (300 K). Brus expanded the Éfros treatment to include screened Coulomb attraction between the two charges, which is represented by the third term in Equation 6 [30]. The associated constant in this term is obtained by averaging the Coulomb interaction over the ground state wavefunction for both particles. The fourth and final term in Equation 6 is the spatial correlation energy between the two particles, a remnant of the exciton effect. It accounts for only a small portion of the total energy [31]. First-principle calculations using variational [32] and density-functional [4] models yield results similar to Equation 6.

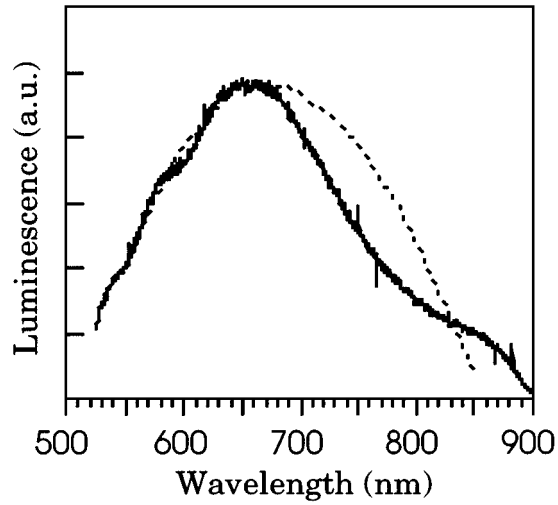

Figure 4 Observed PL from a nanocrystalline germanium sample under laser stimulation.

An example of luminescence observed from a germanium nanocrystal sample at room temperature is shown in Fig. 4. No processing has been done to the raw data. The luminescence spectrum is typically broad in wavelength. This broad band nature is due to the distribution of crystal sizes in the sample film. The films contain many germanium crystals in a range of different sizes, each of which luminesces at a wavelength related to its size. The luminescence is attributed to the nanocrystals, since no luminescence was seen from control films with no germanium or from unannealed films. The luminescence is not due to defect centres in the oxide, which would be passivated by the hydrogen annealing atmosphere [33].

For the sample exhibited in Fig. 4, the peak luminescence is 655 nm. This corresponds to a transition energy of 1.89 eV, considerably shifted from the bulk germanium band gap of 0.67 eV. Also plotted as a dotted line in Fig. 4 is the expected luminescence from a distribution of germanium nanocrystals with similar size and distribution, based on the theory of Equation 6 with no adjustible parameters. Fig. 5 shows the luminescence

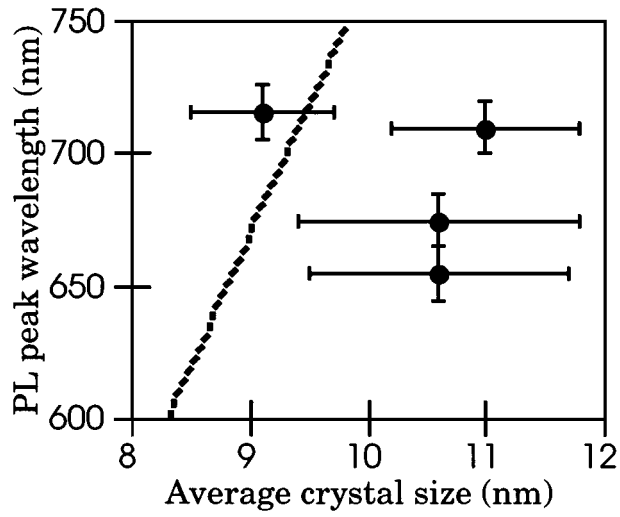

Figure 5 PL peak wavelength as a function of average crystal size (measured from TEM micrographs). The dashed line represents the theoretical luminescence versus size relationship.

peak wavelength plotted against average crystal size for those samples measured by TEM. Also plotted in Fig. 5 is the expected peak luminescence based on Equation 6 with $\mu = 0.02$.

The experimental data match the theoretical luminescence for electron–light hole recombination reasonably well. This agreement provides evidence for quantum confinement as the mechanism responsible for germanium nanocrystal luminescence. The crystal sizes from which luminescence have been observed are 6–10 nm, which is larger than the 5–6 nm maximum size for luminescence predicted by other models [12, 17].

4. Conclusions

We have studied the formation of germanium nanocrystals in a SiO_2 matrix and examined their luminescence properties. The precipitation of nanocrystals does not follow the Lifshitz–Slezov theory. Instead, nanocrystal growth appears to be determined primarily by anneal temperature, with little anneal time dependence. We attribute this departure from theory to the high concentration of germanium in the deposited films. Furthermore, the distribution of nanocrystal sizes is not the distribution predicted by Lifshitz–Slezov. A modified log-normal distribution was found to describe the size distribution best. The nanocrystals from which luminescence is observed are in the bulk diamond phase, in contrast to the claims of other researchers.

The PL spectra observed from germanium nanocrystal samples were broad, in accordance with the distribution of nanocrystal sizes. We have compared the observed PL with measured germanium nanocrystal size. The peak luminescence wavelengths are in agreement with the theory of Brus for quantum confined carriers in small semiconductor crystals. PL from germanium nanocrystals therefore seems consistent with a quantum confinement mechanism.

References

1. S. HAYASHI, T. NAGAREDA, Y. KANAZAWA and K. YAMAMOTO, *Jpn. J. Appl. Phys.* **32** (1993) 3840.
2. H. TAKAGI, H. OGAWA, Y. YAMAZAKI, A. ISHIZAKI and T. NAKAGIRI, *Appl. Phys. Lett.* **56** (1990) 2379.
3. M. YAMAMOTO, R. HAYASHI, K. TSUNETOMO, K. KOHNO and Y. OSAKA, *Jpn. J. Appl. Phys.* **30** (1991) 136.
4. B. DELLEY and E. F. STEIGMEIER, *Phys. Rev. B* **47** (1993) 1397.
5. Y. KANEMITSU, K. SUZUKI, H. UTO, Y. MASUMOTO, T. MATSUMOTO, S. KYUSHIN, K. HIGUCHI and H. MATSUMOTO, *Appl. Phys. Lett.* **61** (1992) 2446.
6. J. P. PROOT, C. DELERUE and G. ALLAN, *ibid.* **61** (1992) 1948.
7. R. HAYASHI, M. YAMAMOTO, K. TSUNETOMO, K. KOHNO, Y. OSAKA and H. NASU, *Jpn. J. Appl. Phys.* **29** (1990) 756.
8. D. C. PAINE, C. CARAGIANIS, T. Y. KIM, Y. SHIGESATO and T. ISHAHARA, *Appl. Phys. Lett.* **62** (1993) 2842.
9. Y. MAEDA, N. TSUKAMOTO, Y. YAZAWA, Y. KANEMITSU and Y. MASUMOTO, *ibid.* **59** (1991) 3168.
10. Y. MASUMOTO, in "Microcrystalline Semiconductors, Materials Science and Devices," Boston, 1992, edited by P. M. Fauchet (Materials Research Society, Pittsburgh, PA, 1993) p. 15.
11. S. HAYASHI, M. FUJII and K. YAMAMOTO, *Jpn. J. Appl. Phys.* **28** (1989) L1464.
12. Y. MAEDA, *Phys. Rev. B* **51** (1995) 1658.
13. K. AWAZU, K. WATANABE and H. KAWAZOE, *Jpn. J. Appl. Phys.* **32** (1993) 2746.
14. S. MUNEKUNI, T. YAMANAKA, Y. SHIMOGAICHI, R. TOHMON, Y. OHKI, K. NAGASAWA and Y. HAMA, *J. Appl. Phys.* **68** (1990) 1212.
15. B. E. WARREN, in "X-Ray Diffraction" (Dover, New York, 1969) p. 251.
16. Y. WANG and N. HERRON, *J. Phys. Chem.* **95** (1991) 525.
17. Y. KANEMITSU, H. UTO, Y. MASUMOTO and Y. MAEDA, *Appl. Phys. Lett.* **61** (1992) 2187.
18. Y. MAEDA, H. UTO, Y. KANEMITSU and Y. MASUMOTO, in 1992 International Conference on Solid State Devices and Materials, Tsukuba, 1992, edited by (Komiyama, Tokyo, 1992) p. 379.
19. I. M. LIFSHITZ and V. V. SLEZOV, *Sov. Phys. JETP* **35** (1959) 331.
20. I. M. LIFSHITZ and V. V. SLYOZOV, *J. Phys. Chem. Solids* **19** (1961) 35.
21. B. G. POTTER and J. H. SIMMONS, *Phys. Rev. B* **37** (1988) 10838.
22. P. W. VOORHEES and M. E. GLICKSMAN, *Acta Metall.* **32** (1984) 2013.
23. K. TSUNETOMO, A. KAWABUCHI, H. KITAYAMA, Y. OSAKA and H. NASU, *Jpn. J. Appl. Phys.* **29** (1990) 2481.
24. J. P. WOLFE, *Physics Today* **March** (1982) 46.
25. S. M. SZE, in "Physics of Semiconductor Devices" (Wiley, New York, 1981) p. 850.
26. V. I. SIDOROV and Y. E. POKROVSKII, *Sov. Phys. Semicond.* **6** (1973) 2015.
27. M. ALTARELLI and N. O. LIPARI, *Phys. Rev. Lett.* **36** (1976) 619.
28. T. TAKAGAHARA, *Phys. Rev. B* **36** (1987) 9293.
29. A. L. ÉFROS and A. ÉFROS, *Sov. Phys. Semicond.* **16** (1982) 772.
30. L. E. BRUS, *J. Chem. Phys.* **80** (1984) 4403.
31. Y. KAYANUMA, *Phys. Rev. B* **38** (1988) 9797.
32. H. M. SCHMIDT and H. WELLER, *Chem. Phys. Lett.* **129** (1986) 1986.
33. K. S. MIN, K. V. SHCHEGLOV, C. M. YANG, H. A. ATWATER, M. L. BRONGERSMA and A. POLMAN, *Appl. Phys. Lett.* **68** (1996) 2511.

Received 28 July 1997
and accepted 30 July 1998